SEISMIC PERFORMANCE OF BRIDGES ISOLATED WITH DCFP DEVICES

Available online at www.easdprocedia.org
EASD Procedia EURODYN (2020) 1704-1721

EASD Procedia

EURODYN 2020
XI International Conference on Structural Dynamics
M. Papadrakakis, M. Fragiadakis, C. Papadimitriou (eds.)
Athens, Greece, 23–26 November 2020

SEISMIC PERFORMANCE OF BRIDGES ISOLATED WITH DCFP DEVICES

P. Castaldo[1], G. Amendola[2], D. Gino[3], E. Miceli[4]

[1] Department of Structural, Geotechnical and Building Engineering (DISEG), Politecnico di Torino
Turin, Italy
e-mail: paolo.castaldo@polito.it

[2] Department of Structural, Geotechnical and Building Engineering (DISEG), Politecnico di Torino
Turin, Italy
e-mail: guglielmo.amendola@polito.it

[3] Department of Structural, Geotechnical and Building Engineering (DISEG), Politecnico di Torino
Turin, Italy
e-mail: diego.gino@polito.it

[4] Department of Structural, Geotechnical and Building Engineering (DISEG), Politecnico di Torino
Turin, Italy
e-mail: elena.miceli@studenti.polito.it

Keywords: seismic isolation, double concave friction pendulum (DCFP) isolator, bridge, pier-abutment-deck interaction, non-dimensional form, optimal friction coefficient.

Abstract. *The paper analyzes the influence of double concave friction pendulum (DCFP) isolator properties on the seismic performance of isolated bridges. The behavior of these systems is analyzed by employing an eight-degree-of-freedom model accounting for the first five vibrational modes of the pier and the presence of a rigid abutment, whereas the DCFP isolator behaviour is described combining two single FPSs in series. The uncertainty in the seismic input is taken into account by considering a set of natural records with different characteristics. The variation of the statistics of the response parameters relevant to the seismic performance is investigated through an extensive parametric study carried out for different system properties.*

ISSN:2311-9020
Peer-review under responsibility of the Organizing Committee of EURODYN 2020.
doi: 10.47964/1120.9137.20045

1 INTRODUCTION

Seismic isolation has emerged as one of the most powerful techniques in the ensemble of retrofitting methodologies [1]-[5] to improve the safety and resilience of infrastructure systems [6]-[7]. In the more general seismic approach, seismic isolation of bridges permits to obtain the uncoupling of the deck from the horizontal earthquake's components, leading to a significant reduction of the deck acceleration and, as consequence, of the forces transmitted to the pier.

Several studies [1]-[4] have been carried out in the last decades investigating the effectiveness of the isolation devices and carrying out experimental and analytical studies on the seismic response of bridges isolated by sliding isolation systems finding out as these kind of devices are quite effective and efficiency in the aseismic bridges' design. Ghobarah and Ali [5] and Turkington et al. [8] showed that the presence of lead-rubber bearings shift the natural period of the structure and increases the amount of damping, moreover they permit to distribute the seismic forces approximately evenly between pier and abutment. Jangid [9] studied the seismic response of bridges seismically isolated by lead-rubber bearings (L-RB) to bidirectional earthquakes outlining that the bidirectional interaction of the restoring forces of the L-RB has not negligible effects on the seismic response of the isolated bridges. In [10]-[11], the seismic behaviour of bridges seismically isolated by adopting friction pendulum system (FPS) was studied. When FPS bearings are used, the natural period of the isolated structure becomes independent of the mass of the superstructure and it just has a dependence on the radius of curvature of the sliding surface [12].

Another important feature of this isolation system is mainly related to the energy dissipation mechanism that becomes possible thanks to the velocity dependent friction between the sliding surfaces and the composite material on the slider [13]-[17]. In addition, it has been demonstrated in [18]-[19] that the characteristics of an FPS become more effective by introducing a second sliding surface obtaining the so called double concave friction pendulum (DCFP). In particular, Kim and Yun [20] studied the positive effects of a double concave friction pendulum system on a bridge response considering different combinations of radii of curvature and of friction coefficients.

Other studies [21]-[22] have been more oriented to define design approaches by means of the seismic reliability-based design (SRBD), in which the main uncertainties such as the seismic input and the system properties have been taken into account. In [23] the optimal properties of FPS able to minimize the seismic response of bridge under earthquake having different frequency contents representative of different soil conditions has been evaluated.

This study analyzes the influence of the double concave friction pendulum (DCFP) isolator properties on the seismic performance of isolated bridges taking into account the pier-abutment-deck interaction. The behavior of these systems, as also described in [10]-[24] is analyzed by employing an eight-degree-of-freedom (8dof) model representative of the reinforced-concrete pier flexibility in addition to the presence of a rigid abutment and deck, whereas the DCFP isolator behaviour is described combining two single FPSs in series [18]-[19]. For each sliding surface, a widespread model which considers the variation of the friction coefficient with the sliding velocity is adopted [15]-[16]. The uncertainty in the seismic input is taken into account by means of a set of natural records with different characteristics. The variation of the statistics of the response parameters relevant to the seismic performance of the isolated bridges is investigated through a nondimensionalization of the motion equations, as also implemented in [25]-[28] developing an extensive parametric study.

2 EQUATIONS OF MOTION

An 8-degree-of-freedom (dof) system is employed to model the isolated bridge configuration of Figure 1. Specifically, 5 dof are given by the lumped masses of the pier, 2 dof correspond to the two slider masses of the DCFP isolators, located respectively on the pier and on the abutment, and 1 dof is related to the rigid deck mass [10].

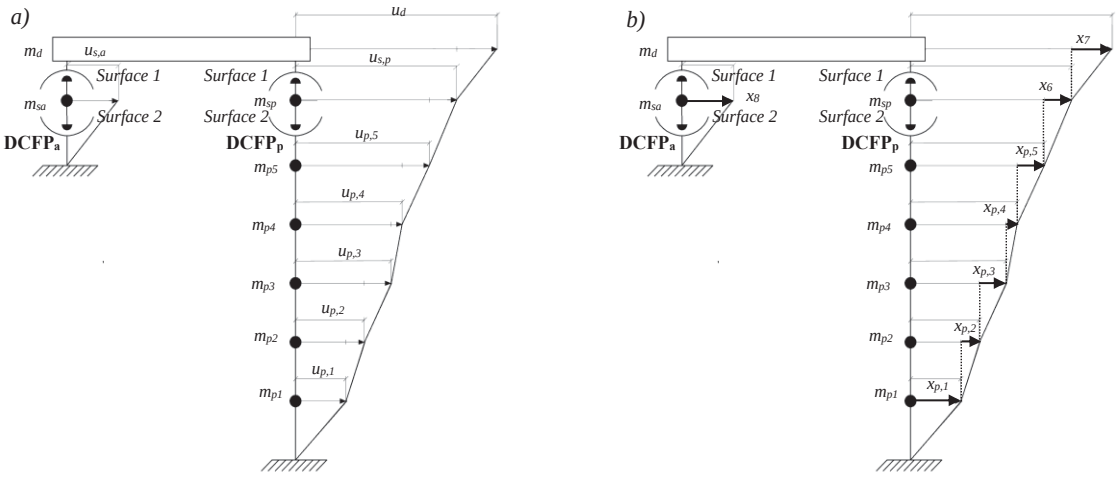

Figure 1: 8dof model of bridge isolated with DCFP bearings: relative displacements with respect to the ground a) and drifts between masses b) .

The equations of motion governing the response of the model representing a bridge on DCFP isolators, in terms of relative displacement with respect to the ground (Figure 1a) subjected to the seismic input $\ddot{u}_g(t)$ is:

$$m_{\mathrm{d}}\left[\ddot{u}_d(t)+\ddot{u}_g(t)\right]+F_{1a}(t)+F_{1p}(t)=0$$

$$m_{sa}\left[\ddot{u}_{sa}(t)+\ddot{u}_g(t)\right]-F_{1a}(t)+F_{2a}(t)=0$$

$$m_{sp}\left[\ddot{u}_{\mathrm{sp}}(t)+\ddot{u}_g(t)\right]-F_{1p}(t)+F_{2p}(t)=0 \qquad \text{(1a,b,c,d,e)}$$

$$m_{p5}\left[\ddot{u}_{p5}(t)+\ddot{u}_g(t)\right]+c_{p5}\left[\dot{u}_{p5}(t)-\dot{u}_{p4}(t)\right]+k_{p5}\left[u_{p5}(t)-u_{p4}(t)\right]-F_{2p}(t)=0$$

$$m_{pi}\left[\ddot{u}_{pi}(t)+\ddot{u}_g(t)\right]+c_{pi}\left[\dot{u}_{pi}(t)-\dot{u}_{pi-1}(t)\right]+k_{pi}\left[u_{pi}(t)-u_{pi-1}(t)\right]+$$
$$-c_{pi+1}\left[\dot{u}_{pi+1}(t)-\dot{u}_{pi}(t)\right]-k_{pi+1}\left[u_{pi+1}(t)-u_{pi}(t)\right]=0 \quad \textit{for} \quad i=1,\ldots,4$$

where u_d denotes the displacement of the superstructure relative to the ground, u_{sp} the displacement of the slider of the DCFP device on the pier with respect to the ground, u_{sa} the displacement of the slider of the DCFP device on the abutment with respect to the ground, u_{pi} (i=1,..,4,5) the displacement of pier i-th mass relative to the ground, m_d , m_{sp} and m_{sa} respectively the mass of the deck and of the two DCFP devices respectively on the pier and on the

abutment, m_{pi} (i=1,..,4,5) the mass the i-th lumped mass of the pier, k_{pi} and c_{pi} (i=1,..,4,5) respectively the stiffness and inherent viscous damping constant for each dof of the pier, t the time instant, the dot differentiation over time, $F_{ja}(t)$ and $F_{jp}(t)$ denote the reaction of the DCFP bearings on the abutment and on the pier, respectively, for the upper (j = *1*) and lower surface (j = *2*). The deck isolated by DCFP isolators is herein considered without any viscous capacities [28].
A DCFP can be modeled as a serial combination of two single FPS. Thus, according with [18]-[19], when the inertial force associated with the movement of the small slider mass is neglected, the reaction forces (F_2 and F_1) at the lower and upper surface become the same and can be readily obtained as follows:

$$F = F_1 = F_2 = \frac{m_d g}{R_1 + R_2}(u) + \frac{m_d g\left(R_1 \mu_1(\dot{u}_1)\operatorname{sgn}(\dot{u}_1) + R_2 \mu_2(\dot{u}_2)\operatorname{sgn}(\dot{u}_2)\right)}{R_1 + R_2} \tag{2}$$

where u is related to the total deformation of the double concave friction pendulum, u_1 to the deformation of the upper surface and u_2 to the lower one. The first part of the right hand side of Eq.s (2) represents the restoring stiffness (k_{comb}) of the combined DCFP from which the restoring natural period can be obtained as follows:

$$k_{comb} = \frac{m_d g}{R_1 + R_2} \tag{3}$$

$$T_d = 2\pi\sqrt{(R_1 + R_2)/g} \tag{4}$$

where g is the gravity constant, R_1 and R_2 are the radii of curvature of the DCFP.

In Eq.(2), $f_j(\dot{u}_j(t))$ (j=*1,2*) is the coefficient of sliding friction, which depends on the slider slip velocity along one of the two bearing internal surfaces, indicated with $\dot{u}_j(t)$, and $\operatorname{sgn}(\dot{u}_j)$ (j=*1,2*) with *sgn*(·) denoting the sign function. Note that the subscript 1 refers to the upper surface whereas the subscript 2 refers to the lower surface. On the other hand, the second part of the Eq.s (2a,b), under the hypothesis that sliding occurs on both surfaces and in the same direction, represents the equivalent friction coefficient of the DCFP [18]:

$$\mu_{eqv} = \frac{\mu_1 R_1 + \mu_2 R_2}{R_1 + R_2} \tag{5}$$

In the above discussion, it is also assumed that the DCFP bearings used to isolate the deck and placed, respectively, on the pier and on the abutment have the same characteristics, so that it's obvious they move simultaneously.
Moreover, experimental results [14]-[16] suggest that, for each sliding surface, the coefficient of sliding friction of Teflon-steel interfaces obeys to the following equation:

$$\mu_j(\dot{u}_j) = \mu_{j,\max} - (\mu_{j,\max} - \mu_{j,\min}) \cdot \exp(-\alpha|\dot{u}_j|) \quad for \quad j = 1,2 \tag{6}$$

in which $\mu_{j,\max}$ represents the maximum value of friction coefficient attained at large velocities of sliding, and $\mu_{j,\min}$ represents the value at zero velocity. To further simplify the problem,

in the following analyses it is assumed that $\mu_{j,\max} = 3\mu_{j,\min}$ based on a regression of the experimental results, whereas the exponent α is assumed equal to 30 [14]-[16].

3 NON-DIMENSIONALIZATION OF THE EQUATIONS OF MOTION

In order to analyze the role of each characteristic parameter controlling the seismic behaviour of the system under investigation, the results obtained solving the equations of motion are reduced to a non-dimensional form as discussed in [26]-[28].
To easily obtain the deformation of the isolators along each sliding surface, Eq.(1) can be rewritten in terms of drifts between the masses of the system instead of displacement respect to the ground:

$$m_d\ddot{x}_7(t)+m_d\ddot{x}_6(t)+m_d\ddot{x}_{p5}(t)+m_d\ddot{x}_{p4}(t)+m_d\ddot{x}_{p3}(t)+m_d\ddot{x}_{p2}(t)+$$
$$+m_d\ddot{x}_{p1}(t)+c_d\dot{x}_d(t)+F_{1a}(t)+F_{1p}(t)=-m_d\ddot{u}_g(t)$$

$$m_{sp}\ddot{x}_6(t)+m_{sp}\ddot{x}_{p5}(t)+m_{sp}\ddot{x}_{p4}(t)+m_{sp}\ddot{x}_{p3}(t)+m_{sp}\ddot{x}_{p2}(t)+$$
$$+m_{sp}\ddot{x}_{p1}(t)-F_{1p}(t)+F_{2p}(t)=-m_{sp}\ddot{u}_g(t)$$

$$m_{sa}\ddot{x}_8(t)-F_{1a}(t)+F_{2a}(t)=-m_{sa}\ddot{u}_g(t)$$

$$m_{p5}\ddot{x}_{p5}(t)+m_{p5}\ddot{x}_{p4}(t)+m_{p5}\ddot{x}_{p3}(t)+m_{p5}\ddot{x}_{p2}(t)+m_{p5}\ddot{x}_{p1}(t)-c_d\dot{x}_d(t)+$$
$$+c_{p5}\dot{x}_{p5}(t)+k_{p5}x_{p5}(t)-F_{2p}(t)=-m_{p5}\ddot{u}_g(t)$$

$$m_{p4}\ddot{x}_{p4}(t)+m_{p4}\ddot{x}_{p3}(t)+m_{p4}\ddot{x}_{p2}(t)+m_{p4}\ddot{x}_{p1}(t)-c_{p5}\dot{x}_{p5}(t)-k_{p5}x_{p5}(t)+$$
$$+c_{p4}\dot{x}_{p4}(t)+k_{p4}x_{p4}(t)=-m_{p4}\ddot{u}_g(t)$$

$$m_{p3}\ddot{x}_{p3}(t)+m_{p3}\ddot{x}_{p2}(t)+m_{p3}\ddot{x}_{p1}(t)-c_{p4}\dot{x}_{p4}(t)-k_{p4}x_{p4}(t)+$$
$$+c_{p3}\dot{x}_{p3}(t)+k_{p3}x_{p3}(t)=-m_{p3}\ddot{u}_g(t) \qquad \text{(7a,b,c,d,e,f,g,h)}$$

$$m_{p2}\ddot{x}_{p2}(t)+m_{p2}\ddot{x}_{p1}(t)-c_{p3}\dot{x}_{p3}(t)-k_{p3}x_{p3}(t)+c_{p2}\dot{x}_{p2}(t)+k_{p2}x_{p2}(t)=-m_{p2}\ddot{u}_g(t)$$

$$m_{p1}\ddot{x}_{p1}(t)-c_{p2}\dot{x}_{p2}(t)-k_{p2}x_{p2}(t)+c_{p1}\dot{x}_{p1}(t)+k_{p1}x_{p1}(t)=-m_{p1}\ddot{u}_g(t)$$

where:

$$F_{1a}=\frac{m_d g}{2}\left[\frac{1}{R_{1a}}\left(\sum_{i=1}^{5}x_{pi}+x_6+x_7-x_8\right)+\mu_{1a}\left(\operatorname{sgn}\left(\sum_{i=1}^{5}\dot{x}_{pi}+\dot{x}_6+\dot{x}_7-\dot{x}_8\right)\right)\right]$$
$$F_{2a}=\left(\frac{m_d}{2}+m_{sa}\right)g\left[\frac{1}{R_{2a}}(x_8)+\left(\mu_{2a}(\dot{x}_8)\right)\left(\operatorname{sgn}(\dot{x}_8)\right)\right] \qquad \text{(8a,b,c,d)}$$
$$F_{1p}=\left(\frac{m_d g}{2}\right)\left[\frac{1}{R_{1p}}(x_7)+\left(\mu_{1p}(\dot{x}_7)\right)\left(\operatorname{sgn}(\dot{x}_7)\right)\right]$$
$$F_{2p}=\left(\frac{m_d}{2}+m_{sp}\right)g\left[\frac{1}{R_{2p}}(x_6)+\left(\mu_{2p}(\dot{x}_6)\right)\left(\operatorname{sgn}(\dot{x}_6)\right)\right]$$

After that, dividing all the equations by m_d, Eq.(7) applies:

$$\ddot{x}_7(t)+\ddot{x}_6(t)+\ddot{x}_{p5}(t)+\ddot{x}_{p4}(t)+\ddot{x}_{p3}(t)+\ddot{x}_{p2}(t)+\ddot{x}_{p1}(t)+2\xi_d\omega_d\dot{x}_d(t)+$$
$$+\frac{g}{2}\left[\frac{1}{R_{1a}}\left(\sum_{i=1}^{5}x_{pi}+x_6+x_7-x_8\right)+\mu_{1a}(v)\left(\operatorname{sgn}\left(\sum_{i=1}^{5}\dot{x}_{pi}+\dot{x}_6+\dot{x}_7-\dot{x}_8=v\right)\right)\right]+$$
$$+\frac{g}{2}\left[\frac{1}{R_{1p}}(x_7)+\left(\mu_{1p}(\dot{x}_7)\right)\left(\operatorname{sgn}(\dot{x}_7)\right)\right]=\ddot{u}_g(t)$$

$$\lambda_{sp}\left(\ddot{x}_6(t)+\ddot{x}_{p5}(t)+\ddot{x}_{p4}(t)+\ddot{x}_{p3}(t)+\ddot{x}_{p2}(t)+\ddot{x}_{p1}(t)\right)+$$
$$-\frac{g}{2}\left[\frac{1}{R_{1p}}(x_7)+\left(\mu_{1p}(\dot{x}_7)\right)\left(\operatorname{sgn}(\dot{x}_7)\right)\right]+\left(\frac{1}{2}+\lambda_{sp}\right)g\left[\frac{1}{R_{2p}}(x_6)+\left(\mu_{2p}(\dot{x}_6)\right)\left(\operatorname{sgn}(\dot{x}_6)\right)\right]=-\lambda_{sp}\ddot{u}_g(t)$$

$$\lambda_{sa}\ddot{x}_8(t)-\frac{g}{2}\left[\frac{1}{R_{1a}}\left(\sum_{i=1}^{5}x_{pi}+x_6+x_7-x_8\right)+\mu_{1a}(v)\left(\operatorname{sgn}\left(\sum_{i=1}^{5}\dot{x}_{pi}+\dot{x}_6+\dot{x}_7-\dot{x}_8=v\right)\right)\right]+$$
$$+\left(\frac{1}{2}+\lambda_{sa}\right)g\left[\frac{1}{R_{2a}}(x_8)+\left(\mu_{2a}(\dot{x}_8)\right)\left(\operatorname{sgn}(\dot{x}_8)\right)\right]=-\lambda_{sa}\ddot{u}_g(t)$$

$$\lambda_{p5}\left(\ddot{x}_{p5}(t)+\ddot{x}_{p4}(t)+\ddot{x}_{p3}(t)+\ddot{x}_{p2}(t)+\ddot{x}_{p1}(t)\right)-2\xi_d\omega_d\dot{x}_d(t)+2\xi_{p5}\omega_{p5}\lambda_{p5}\dot{x}_{p5}(t)+\omega_{p5}^2\lambda_{p5}x_{p5}(t)+$$
$$-\left(\frac{1}{2}+\lambda_{sp}\right)g\left[\frac{1}{R_{2p}}(x_6)+\left(\mu_{2p}(\dot{x}_6)\right)\left(\operatorname{sgn}(\dot{x}_6)\right)\right]=-\lambda_{p5}\ddot{u}_g(t)$$

$$\lambda_{p4}\left(\ddot{x}_{p4}(t)+\ddot{x}_{p3}(t)+\ddot{x}_{p2}(t)+\ddot{x}_{p1}(t)\right)-2\xi_{p5}\omega_{p5}\lambda_{p5}\dot{x}_{p5}(t)-\omega_{p5}^2\lambda_{p5}x_{p5}(t)+$$
$$+2\xi_{p4}\omega_{p4}\lambda_{p4}\dot{x}_{p4}(t)+\omega_{p4}^2\lambda_{p4}x_{p4}(t)=-\lambda_{p4}\ddot{u}_g(t)$$

(9a,b,c,d,e,f,g,h)

$$\lambda_{p3}\left(\ddot{x}_{p3}(t)+\ddot{x}_{p2}(t)+\ddot{x}_{p1}(t)\right)-2\xi_{p4}\omega_{p4}\lambda_{p4}\dot{x}_{p4}(t)-\omega_{p4}^2\lambda_{p4}x_{p4}(t)+2\xi_{p3}\omega_{p3}\lambda_{p3}\dot{x}_{p3}(t)+$$
$$+\omega_{p3}^2\lambda_{p3}x_{p3}(t)=-\lambda_{p3}\ddot{u}_g(t)$$

$$\lambda_{p2}\left(\ddot{x}_{p2}(t)+\ddot{x}_{p1}(t)\right)-2\xi_{p3}\omega_{p3}\lambda_{p3}\dot{x}_{p3}(t)-\omega_{p3}^2\lambda_{p3}x_{p3}(t)+2\xi_{p2}\omega_{p2}\lambda_{p2}\dot{x}_{p2}(t)+$$
$$+\omega_{p2}^2\lambda_{p2}x_{p2}(t)=-\lambda_{p2}\ddot{u}_g(t)$$

$$\lambda_{p1}\ddot{x}_{p1}(t)-2\xi_{p2}\omega_{p2}\lambda_{p2}\dot{x}_{p2}(t)-\omega_{p2}^2\lambda_{p2}x_{p2}(t)+2\xi_{p1}\omega_{p1}\lambda_{p1}\dot{x}_{p1}(t)+\omega_{p1}^2\lambda_{p1}x_{p1}(t)=-\lambda_{p1}\ddot{u}_g(t)$$

and the following ratios are introduced:

$$\lambda_{pi}=\frac{m_{pi}}{m_d},\ \lambda_{sa}=\frac{m_{sa}}{m_d},\ \lambda_{sp}=\frac{m_{sp}}{m_d},$$
$$\omega_d=\sqrt{\frac{k_{comb}}{m_d}},\ \omega_{pi}=\sqrt{\frac{k_{pi}}{m_{pi}}},\ \xi_{pi}=\frac{c_{pi}}{2m_{pi}\omega_{pi}} \tag{10a,b,c,d,e,f}$$

where the first three terms are the mass ratios, the third and the fourth terms are the circular frequency of vibration of the isolated deck and of the *i*-th dof of the pier and the one denotes the damping factor of the *i*-th dof of the pier.

Inspired from [26]-[28], let us introduce the time scale $\tau=t\omega_d$ in which ω_d is the fundamental circular frequency of the isolated system with infinitely rigid superstructure, considering

the equivalent stiffness of the DCFP isolator k_{comb}, and the seismic intensity scale a_0, expressed as $\ddot{u}_g(t) = a_0 \ell(\tau)$ where $\ell(\tau)$ is a non-dimensional function of time describing the seismic input time-history, the following non-dimensional equations can be obtained:

$$\ddot{\psi}_7(\tau)+\ddot{\psi}_6(\tau)+\ddot{\psi}_{p5}(\tau)+\ddot{\psi}_{p4}(\tau)+\ddot{\psi}_{p3}(\tau)+\ddot{\psi}_{p2}(\tau)+\ddot{\psi}_{p1}(\tau)+2\xi_d\dot{\psi}_7(\tau)+\frac{g}{2}\left[\frac{1}{R_{1p}}\frac{1}{\omega_d^{\,2}}\psi_7(\tau)+\frac{\mu_{1p}(\dot{\psi}_7)}{a_0}\operatorname{sgn}(\dot{\psi}_7)\right]+$$
$$+\frac{g}{2}\left[\frac{1}{R_{1a}}\frac{1}{\omega_d^{\,2}}\left(\sum_{i=1}^{5}\psi_{pi}(\tau)+\psi_6(\tau)+\psi_7(\tau)-\psi_8(\tau)\right)+\right.$$
$$\left.+\left(\frac{\mu_{1a}}{a_0}\left(\sum_{i=1}^{5}\dot{\psi}_{pi}(t)+\dot{\psi}_6(\tau)+\dot{\psi}_7(\tau)-\dot{\psi}_8(\tau)\right)\right)\left(\operatorname{sgn}\left(\sum_{i=1}^{5}\dot{\psi}_{pi}(\tau)+\dot{\psi}_6(\tau)+\dot{\psi}_7(\tau)-\dot{\psi}_8(\tau)\right)\right)\right]=-\ell(\tau)$$

$$\lambda_{sp}\left[\ddot{\psi}_6(\tau)+\ddot{\psi}_{p5}(\tau)+\ddot{\psi}_{p4}(\tau)+\ddot{\psi}_{p3}(\tau)+\ddot{\psi}_{p2}(\tau)+\ddot{\psi}_{p1}(\tau)\right]-\frac{g}{2}\left[\frac{1}{R_{1p}}\frac{1}{\omega_d^{\,2}}\psi_7(\tau)+\frac{\mu_{1p}(\dot{\psi}_7)}{a_0}\operatorname{sgn}(\dot{\psi}_7)\right]+$$
$$+\left(\frac{1}{2}+\lambda_{sp}\right)g\left[\frac{1}{R_{2p}}\frac{1}{\omega_d^{\,2}}\psi_6(\tau)+\frac{\mu_{2p}(\dot{\psi}_6)}{a_0}\operatorname{sgn}(\dot{\psi}_6)\right]=-\lambda_{sp}\ell(\tau)$$

$$\lambda_{sa}\ddot{\psi}_8(\tau)-\frac{g}{2}\left[\frac{1}{R_{1a}}\frac{1}{\omega_d^{\,2}}\left(\sum_{i=1}^{5}\psi_{pi}(\tau)+\psi_6(\tau)+\psi_7(\tau)-\psi_8(\tau)\right)+\right.$$
$$\left.+\left(\frac{\mu_{1a}}{a_0}\left(\sum_{i=1}^{5}\dot{\psi}_{pi}(t)+\dot{\psi}_6(\tau)+\dot{\psi}_7(\tau)-\dot{\psi}_8(\tau)\right)\right)\left(\operatorname{sgn}\left(\sum_{i=1}^{5}\dot{\psi}_{pi}(\tau)+\dot{\psi}_6(\tau)+\dot{\psi}_7(\tau)-\dot{\psi}_8(\tau)\right)\right)\right]+$$
$$\left(\frac{1}{2}+\lambda_{sa}\right)g\left[\frac{1}{R_{2a}}\frac{1}{\omega_d^{\,2}}\psi_8(\tau)+\frac{\mu_{2a}(\dot{\psi}_8)}{a_0}\operatorname{sgn}(\dot{\psi}_8)\right]=-\lambda_{sa}\ell(\tau)$$

$$\lambda_{p5}\left[\ddot{\psi}_{p5}(\tau)+\ddot{\psi}_{p4}(\tau)+\ddot{\psi}_{p3}(\tau)+\ddot{\psi}_{p2}(\tau)+\ddot{\psi}_{p1}(\tau)\right]-2\xi_d\dot{\psi}_d(\tau)+2\xi_{p5}\lambda_{p5}\frac{\omega_{p5}}{\omega_d}\dot{\psi}_{p5}(\tau)+\frac{\lambda_{p5}\omega_{p5}^2}{\omega_d^2}\psi_{p5}(\tau)+$$
$$-\left(\frac{1}{2}+\lambda_{sp}\right)g\left[\frac{1}{R_{2p}}\frac{1}{\omega_d^{\,2}}\psi_6(\tau)+\frac{\mu_{2p}(\dot{\psi}_6)}{a_0}\operatorname{sgn}(\dot{\psi}_6)\right]=-\lambda_{p5}\ell(\tau)$$

$$\lambda_{p4}\left[\ddot{\psi}_{p4}(\tau)+\ddot{\psi}_{p3}(\tau)+\ddot{\psi}_{p2}(\tau)+\ddot{\psi}_{p1}(\tau)\right]-2\xi_{p5}\lambda_{p5}\frac{\omega_{p5}}{\omega_d}\dot{\psi}_{p5}(\tau)+2\xi_{p4}\lambda_{p4}\frac{\omega_{p4}}{\omega_d}\dot{\psi}_{p4}(\tau)-\lambda_{p5}\frac{\omega_{p5}^2}{\omega_d^2}\psi_{p5}(\tau)+$$
$$+\lambda_{p4}\frac{\omega_{p4}^2}{\omega_d^2}\psi_{p4}(\tau)=-\lambda_{p4}\ell(\tau)$$

$$\lambda_{p3}\left[\ddot{\psi}_{p3}(\tau)+\ddot{\psi}_{p2}(\tau)+\ddot{\psi}_{p1}(\tau)\right]-2\xi_{p4}\lambda_{p4}\frac{\omega_{p4}}{\omega_d}\dot{\psi}_{p4}(\tau)+2\xi_{p3}\lambda_{p3}\frac{\omega_{p3}}{\omega_d}\dot{\psi}_{p3}(\tau)-\lambda_{p4}\frac{\omega_{p4}^2}{\omega_d^2}\psi_{p4}(\tau)+$$
$$+\lambda_{p3}\frac{\omega_{p3}^2}{\omega_d^2}\psi_{p3}(\tau)=-\lambda_{p3}\ell(\tau)$$

$$\lambda_{p2}\left[\ddot{\psi}_{p2}(\tau)+\ddot{\psi}_{p1}(\tau)\right]-2\xi_{p3}\lambda_{p3}\frac{\omega_{p3}}{\omega_d}\dot{\psi}_{p3}(\tau)+2\xi_{p2}\lambda_{p2}\frac{\omega_{p2}}{\omega_d}\dot{\psi}_{p2}(\tau)-\lambda_{p3}\frac{\omega_{p3}^2}{\omega_d^2}\psi_{p3}(\tau)+ \qquad \text{(11 a,b,c,d,e,f,g,h)}$$
$$+\lambda_{p2}\frac{\omega_{p2}^2}{\omega_d^2}\psi_{p2}(\tau)=-\lambda_{p2}\ell(\tau)$$

$$\lambda_{p1}\ddot{\psi}_{p1}(\tau)-2\xi_{p2}\lambda_{p2}\frac{\omega_{p2}}{\omega_d}\dot{\psi}_{p2}(\tau)+2\xi_{p1}\lambda_{p1}\frac{\omega_{p1}}{\omega_d}\dot{\psi}_{p1}(\tau)-\lambda_{p2}\frac{\omega_{p2}^2}{\omega_d^2}\psi_{p2}(\tau)+\lambda_{p1}\frac{\omega_{p1}^2}{\omega_d^2}\psi_{p1}(\tau)=-\lambda_{p1}\ell(\tau)$$

Furthermore, the following non-dimensional parameters that control the bridge system of Figure 1 have been adopted:

$$\Pi_{\omega i}=\frac{\omega_{pi}}{\omega_d},\ \Pi_{\lambda i}=\lambda_{pi}=\frac{m_{pi}}{m_d},\ \Pi_{\lambda sa}=\lambda_{sa},\ \Pi_{\lambda sp}=\lambda_{sp},$$
$$\Pi_{\mu a}\left(\dot{\psi}_d\right)=\frac{\mu_a\left(\dot{\psi}_d\right)g}{a_0},\quad \Pi_{\mu p}\left(\dot{\psi}_d\right)=\frac{\mu_p\left(\dot{\psi}_d\right)g}{a_0},\ \Pi_{\xi_{pi}}=\xi_{pi} \tag{12a,b,c,d,e,f,g}$$

$\Pi_{\lambda,}\,\Pi_{\lambda sa,}\,\Pi_{\lambda sp,}$ are the previously defined mass ratios, Π_{ξ_p} describes the viscous damping inherent respectively to the pier dof. Regarding the control parameters of the pier, indeed, the parameters ω_{pi} are related to the fundamental vibration pulsation ω_p (the first vibration mode) as well as the sum of the mass ratios is related to the overall mass ratio $\Pi_\lambda=\lambda_p=\frac{\sum_{i=1,5} m_{pi}}{m_d}$ and, finally, all the damping factors are assumed equal to $\Pi_{\xi_p}=\xi_p$.

The non-dimensional parameters $\Pi_{\mu a,}\,\Pi_{\mu p}$ measure the isolator strengths, provided by the friction coefficients of the two isolators, respectively. Since these parameters depend on the response through the velocities, the following parameters are used in their steads:

$$\Pi^*_{\mu a}=\frac{\mu_{\max,a}g}{a_0},\quad \Pi^*_{\mu p}=\frac{\mu_{\max,p}g}{a_0} \tag{13a,b}$$

It is important to observe that the normalized response of the dynamic system does not depend on the seismic intensity level a_0. Conversely, the seismic response depends also on the function $\lambda(\tau)$ and also on the isolation circular frequency ω_d (or period $T_d=2\pi/\omega_d$).

The non-dimensional response parameters that describe the dynamic response of the deck and of the *i*-th dof for the pier and the two sliders are, respectively:

$$\psi_{u_d}=\frac{u_{d,\text{peak}}\omega_d^2}{S_A(T_d)}\quad,\ \psi_{x_d}=\frac{x_{d,\text{peak}}\omega_d^2}{S_A(T_d)}=\frac{(x_6+x_7)_{\text{peak}}\omega_d^2}{S_A(T_d)},$$
$$\psi_{u_p}=\frac{u_{p,\text{peak}}\omega_d^2}{S_A(T_d)}=\frac{u_{p5,\text{peak}}\omega_d^2}{S_A(T_d)},\ \psi_{x_i}=\frac{x_{i,\text{peak}}\omega_d^2}{S_A(T_d)}\quad \text{with}\ i=1,\ldots,8 \tag{14a,b,c,d}$$

4 PARAMETRIC STUDY

This section presents the results of an extensive parametric study carried out on the bridge system of Fig. 1 to evaluate the performance of bridges isolated with DCFP bearings.

Seismic input description

The evaluation of the seismic performance of any engineered systems should account for the variability of the intensity, frequency content, and duration of the records at the site. Coherently with the performance-based earthquake engineering (PBEE) approach [29]-[30], this study separates the uncertainties related to the seismic input intensity from those related to the characteristics of the record (record-to-record variability) by introducing a scale factor, a_0, i.e. an intensity measure (*IM)*. By this way, the randomness in the seismic intensity can be described by a hazard curve, whereas the ground motion randomness for a fixed intensity level

can be described by selecting a set of ground motion realizations characterized by a different duration and frequency content, and by scaling these records to the common a_0 value. In line with the criteria of efficiency, sufficiency, and hazard computability [34]-[35], in this study, the spectral pseudo-acceleration, $S_A(T_d)$, at the isolated period of the system, $T_d = 2\pi / \omega_d$, is assumed as intensity measure. This *IM* is related to the spectral displacement S_d by the relation $S_A(T_d) = \omega_d^2 S_d(T_d)$. Many studies (e.g., [34]-[35]) demonstrated that S_A is more efficient than the peak ground acceleration, and its use permits to reduce the response dispersion for the same number of ground motion considered and to obtain more confident response estimates for a given number of records employed.

#	Year	Earthquake Name	Recording Station Name	Vs_{30} [m/sec]	Source (Fault Type)	M [-]	R [km]	PGA_{max} [g]
1	1994	Northridge	Beverly Hills - Mulhol	356	Thrust	6.7	13.3	0.52
2	1994	Northridge	Canyon Country-WLC	309	Thrust	6.7	26.5	0.48
3	1994	Northridge	LA – Hollywood Stor	316	Thrust	6.7	22.9	0.36
4	1999	Duzce, Turkey	Bolu	326	Strike-slip	7.1	41.3	0.82
5	1999	Hector Mine	Hector	685	Strike-slip	7.1	26.5	0.34
6	1979	Imperial Valley	Delta	275	Strike-slip	6.5	33.7	0.35
7	1979	Imperial Valley	El Centro Array #11	196	Strike-slip	6.5	29.4	0.38
8	1995	Kobe, Japan	Nishi-Akashi	609	Strike-slip	6.9	8.7	0.51
9	1995	Kobe, Japan	Shin-Osaka	256	Strike-slip	6.9	46	0.24
10	1999	Kocaeli, Turkey	Duzce	276	Strike-slip	7.5	98.2	0.36
11	1999	Kocaeli, Turkey	Arcelik	523	Strike-slip	7.5	53.7	0.22
12	1992	Landers	Yermo Fire Station	354	Strike-slip	7.3	86	0.24
13	1992	Landers	Coolwater	271	Strike-slip	7.3	82.1	0.42
14	1989	Loma Prieta	Capitola	289	Strike-slip	6.9	9.8	0.53
15	1989	Loma Prieta	Gilroy Array #3	350	Strike-slip	6.9	31.4	0.56
16	1990	Manjil, Iran	Abbar	724	Strike-slip	7.4	40.4	0.51
17	1987	Superstition Hills	El Centro Imp. Co.	192	Strike-slip	6.5	35.8	0.36
18	1987	Superstition Hills	Poe Road (temp)	208	Strike-slip	6.5	11.2	0.45
19	1987	Superstition Hills	Westmorland Fire Stat.	194	Strike-slip	6.5	15.1	0.21
20	1992	Cape Mendocino	Rio Dell Overpass	312	Thrust	7.0	22.7	0.55
21	1999	Chi-Chi, Taiwan	CHY101	259	Thrust	7.6	32	0.44
22	1999	Chi-Chi, Taiwan	TCU045	705	Thrust	7.6	77.5	0.51
23	1971	San Fernando	LA - Hollywood Stor	316	Thrust	6.6	39.5	0.21
24	1976	Friuli, Italy	Tolmezzo	425	Thrust	6.5	20.2	0.35
25	1980	Irpinia	Bisaccia	496		6.9	21.3	0.94
26	1979	Montenegro	ST64	1083	Thrust	6.9	21.0	0.18
27	1997	Umbria Marche	ST238	n/a	Normal	6.0	21.5	0.19
28	2000	South Iceland	ST2487	n/a	Strike-slip	6.5	13	0.16
29	2000	South Iceland (a.s.)	ST2557	n/a	Strike-slip	6.5	15.0	0.13
30	2003	Bingol	ST539	806	Strike-slip	6.3	14.0	0.30

Table 1. Selected ground motions for time history analysis.

In this specific study, the choice of $S_A(T_d)$ as *IM* is motivated by the fact that if all the records are normalized to $S_A(T_d)$, then the normalized displacement response of a system with

period T_d, rigid superstructure and mounted on a frictionless isolator is equal to 1 for each record and it is not affected by the record-to-record variability. Thus, this system can be assumed as reference case for evaluating the influence of the isolator friction and of the isolation period on the response statistics. The record-to-record variability is described through a set of 30 real ground motion records reported in Table 1.

Seismic performance description

This study considers the following set of response parameters relevant to the performance of the isolated system (Eq. (10)): the peak isolator deformation between the two devices $u_{d,\max}$ and $x_{d,\max}$, the peak displacement of pier's top relative to the ground $u_{p,\max}$ and the peak relative displacement along the pier $x_{pi,\max}$. These parameters have be expressed in non-dimensional form according to Eq.s (11) and (13).
By repeatedly solving Eqn. (9) for the ground motions records reported in Table 1, a set of samples is obtained for each output variable used to monitor the seismic performance.
In this paper, the response parameters are assumed to follow a lognormal distribution as widely employed in PBEE [29]-[30] and in many parametric studies concerning the performance of structural systems also since the log-normality assumption permits to estimate, with a limited number of samples, the response at different percentile levels, which is very useful for system reliability assessment [25],[31]-[41].
A lognormal distribution can be fitted to the generic response parameter *D* (i.e., the extreme values $\psi_{u_d}, \psi_{x_d}, \psi_{u_p}$, ψ_{x_i} of Eq.s (11) and (12) by estimating the sample geometric mean, $GM\left(D\right)$, and the sample dispersion, $\beta\left(D\right)$, defined as follows:

$$GM\left(D\right) = \sqrt[N]{d_1 \cdot \ldots \cdot d_N} \tag{15}$$

$$\beta\left(D\right) = \sigma_{\ln}\left(D\right) = \sqrt{\frac{\left(\ln d_1 - \ln\left[GM\left(D\right)\right]\right)^2 + \ldots\ldots + \left(\ln d_N - \ln\left[GM\left(D\right)\right]\right)^2}{N-1}} \tag{16}$$

where d_i denotes the *i*-th sample value of *D*, and *N* is the total number of samples. The sample geometric mean is an estimator of the median of the response and its logarithm coincides with the lognormal sample mean $\mu_{\ln}\left(D\right)$ [26].

Parametric study results

This section shows the results of the parametric study carried out to evaluate the relation between the isolation and bridge properties and the system performance, for the reference seismic input described through the ground motion records of Table 1.
Note that any model uncertainty is considered in the numerical analyses [43]-[45]. The configuration of Table 2 has been used for the DCFP bearings properties.
The two DCFP devices on the abutment and on the pier are identical. So, it follows that $\Pi^*_{\mu a} = \Pi^*_{\mu p} = \Pi^*_{\mu}$ as well as $\Pi_{\lambda sa} = \Pi_{\lambda sp} = \Pi_{\lambda s}$. The parameter $\Pi_{\xi_p} = \xi_p$ is assumed equal to 5%, the isolated bridge period T_d is varied in the range between 2s, 2.5s, 3s, 3.5s and 4s, the pier period T_p in the range between 0.05s, 0.1s, 0.15s and 0.2s. Assuming that each of the pier masses are equal, $\Pi_{\lambda} = \lambda_p$ has been considered varying in the range between 0.1, 0.15 and 0.2, Π^*_{μ} in the range between 0 (no friction) and 2 (very high friction). For numerical reasons, the

ratio $\Pi_{\lambda s}$ is assumed equal to 0.005. Therefore, numerical investigations have been carried out on several different systems by varying the main dynamic parameters and for two different DCFP bearing configurations for 30 different time history seismic input.
For each value of the parameters of interest in the parametric study, the differential equation of motion, i.e., Eqn. (9), has been repeatedly solved for the different ground motion considered. The Bogacki-Shampine integration algorithm available in Matlab-Simulink [42] has been employed choosing a variable step to improve the solution accuracy. The probabilistic properties of the normalized response have been evaluated by estimating the geometric mean, *GM*, and the dispersion, β, of the parameters of interest through Eqns. (15) and (16).

	R_1/R_2	$\mu_{1,max}/\ \mu_{2,max}$	μ_{eqv}
Case 1	2	4	3 μ_2

Table 2. DCFP bearings properties within the parametric analysis.

Figs. 2-5 show the statistics (*GM* and β values) of the response parameters considered, obtained for different values of the system parameters varying in the range of interest. Each figure contains three surface plots, corresponding to different values of Π_λ. Only the results corresponding to T_p= 0.1s and T_p= 0.2s are illustrated.

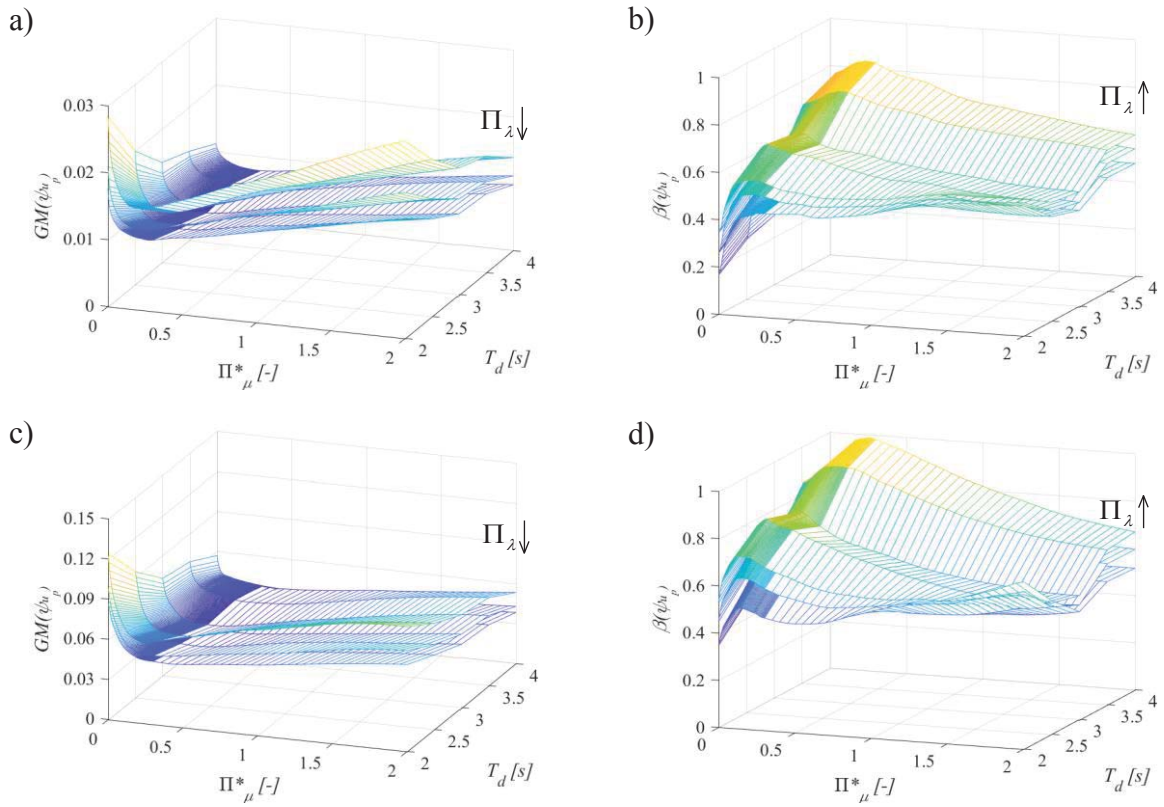

Figure 2. Normalized displacement of pier top vs. Π^*_μ and T_d: median value and dispersion for T_p = 0.1s (a and b) and T_p = 0.2s (c and d) for different values of Π_λ. The arrow denotes the increasing direction of Π_λ.

Fig. 2 plots the results concerning the normalized displacement of pier top ψ_{u_p} with respect to the ground. It is noteworthy that for very low Π_μ^* values, $GM\left(\psi_{u_p}\right)$ decreases by increasing Π_μ^*, whereas for high Π_μ^* values it increases by increasing Π_μ^*. Thus, there exists an optimal value of Π_μ^* such that the displacement of pier top is minimized. This critical value is in the range between 0 and 0.5 depending on the values of T_d, T_p and Π_λ. In addition to that, $GM\left(\psi_{u_p}\right)$ decreases significantly with increasing Π_λ and decreasing T_p, which control directly the main modal period of the pier (for higher ω_d^2, smaller will be the displacement of the pier top). T_d has an influence on $GM\left(\psi_{u_p}\right)$ leading to a general decrease for its increase. The dispersion $\beta\left(\psi_{u_p}\right)$ shows a maximum value approximatively at the same value of Π_μ^* that gives the minimum value of $GM\left(\psi_{u_p}\right)$. The response dispersion increases with increasing vibration period T_p and mass ratio Π_λ. From low to high values of T_d, the dispersion $\beta\left(\psi_{u_p}\right)$ tends to increase.

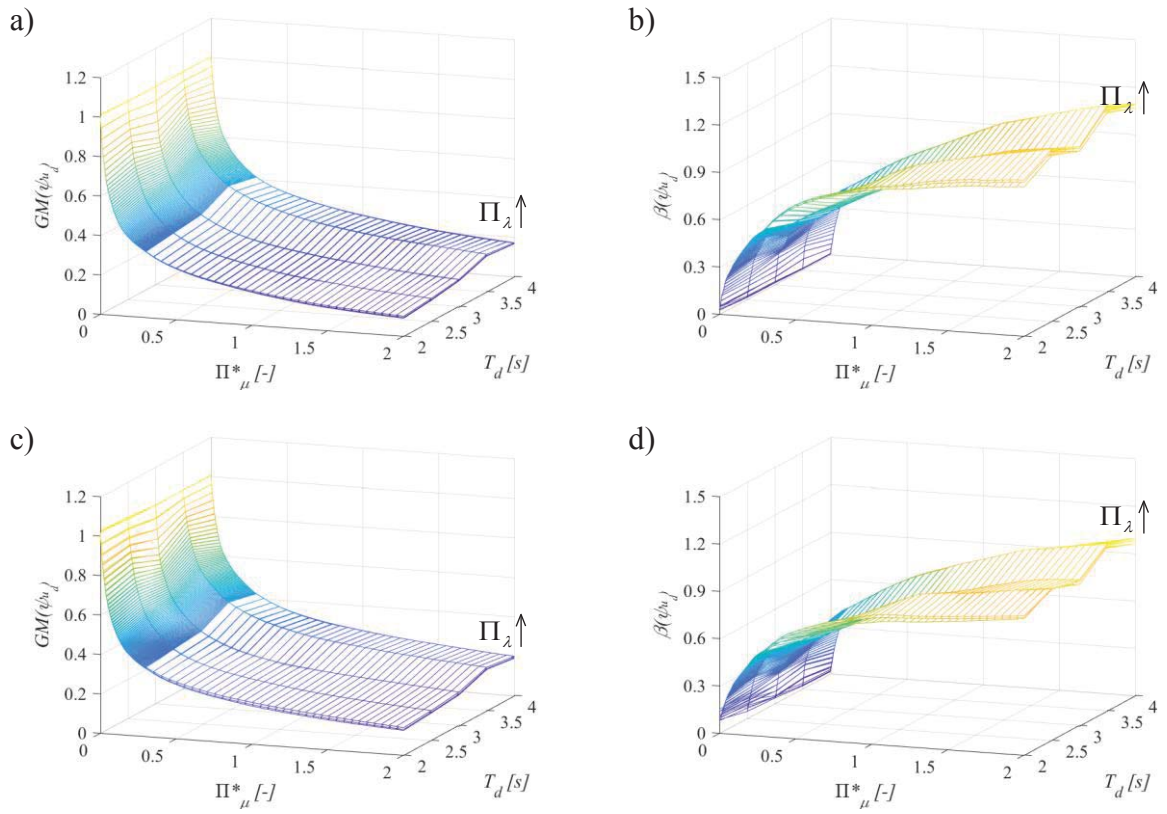

Figure 3. Normalized deck displacement vs. Π^*_μ and T_d: median value and dispersion T_p = 0.1s (a and b) and T_p = 0.2s (c and d) for different values of Π_γ. The arrow denotes the increasing direction of Π_γ.

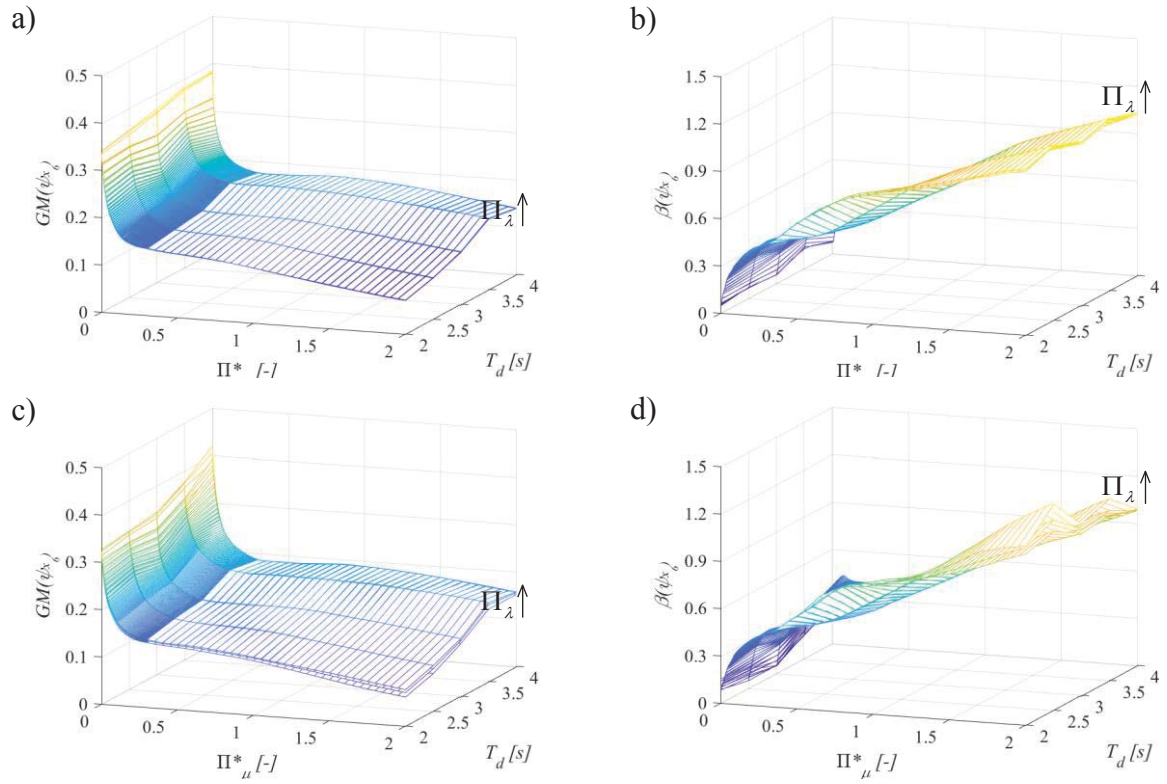

Figure 4. Normalized pier bearing deformation along the lower surface vs. Π^*_μ and T_d: median value and dispersion for T_p = 0.1s (a and b) and T_p = 0.2s (c and d) for different values of Π_λ. The arrow denotes the increasing direction of Π_λ.

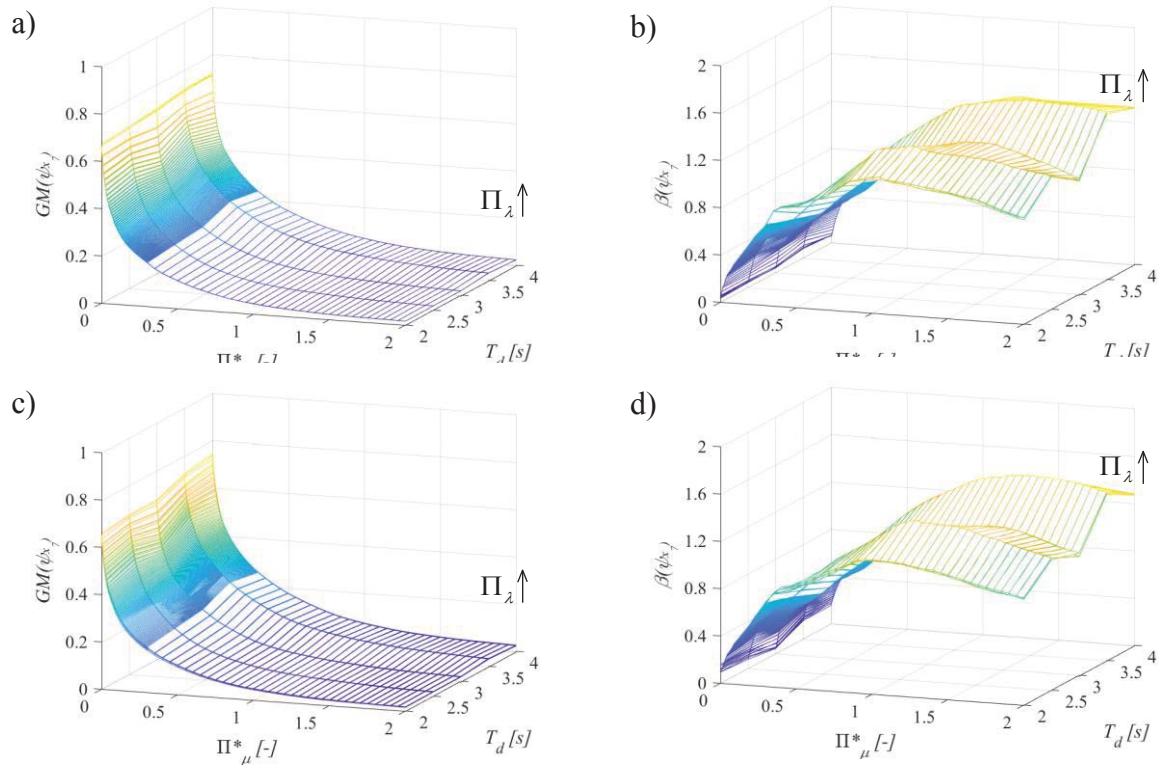

Figure 5. Normalized pier bearing deformation along the upper surface vs. Π^*_μ and T_d: median value and dispersion for T_p = 0.1s (a and b) and T_p = 0.2s (c and d) for different values of Π_λ. The arrow denotes the increasing direction of Π_λ.

Fig. 3 (a,c) shows the response statistics of the normalized deck displacement ψ_{u_d}, which corresponds to the overall deformation of the bearing placed on the abutment, since this latter is the peak value with respect to the displacement relative to the pier top of the other device due to the flexibility of the pier. Obviously, $GM\left(\psi_{u_d}\right)$ decreases significantly as Π^*_μ increases. In general, the values of $GM\left(\psi_{u_d}\right)$ increase slightly for increasing values of T_d and of Π_λ, and they are not affected significantly by T_p. The values of the dispersion $\beta\left(\psi_{u_d}\right)$, plotted in Figs. 3(b,d), are very low for low Π^*_μ values due to the high efficiency of the *IM* employed in the study, and attain their peak for high values of Π^*_μ. The other system parameters have a reduced influence on $\beta\left(\psi_{u_d}\right)$ compared to the influence of Π^*_μ.

Fig. 4(a) and (c) show the variation with the system parameters of the geometric mean of the normalized pier bearing deformation along the lower surface $GM(\psi_{x_6})$, for T_p=0.1s and T_p=0.2s. This parameter decreases at first quickly, and then slightly increases after values of Π^*_μ close to 0.5, reaching a maximum for Π^*_μ close to 1. The values of the dispersion $\beta\left(\psi_{x_6}\right)$, plotted in Figs. 4 (b,d), are very low for low Π^*_μ values, and increase monotonically with Π^*_μ. The other system parameters have a negligible influence on $\beta\left(\psi_{x_6}\right)$ compared to the influence of Π^*_μ.

Fig. 5(a) and (c) show the variation with the system parameters of the geometric mean of the normalized pier bearing deformation along the upper surface $GM(\psi_{x_7})$, for T_p = 0.1s and T_p = 0.2s. This parameter decreases hyperbolically with increasing Π^*_μ. The values of the dispersion $\beta\left(\psi_{x_7}\right)$, plotted in Figs. 5(b,d), are very low for low Π^*_μ values, and show a maximum for $\Pi^*_\mu \approx 1$, reaching very high values close to 1.5. Once again, the other system parameters have a no significant influence on $\beta\left(\psi_{x_7}\right)$ compared to the influence of Π^*_μ.

These last figures demonstrate the highest influence of the upper surface, characterized by higher values of the sliding friction coefficient and of the radius of curvature to define the global response of the seismic DCFP device as shown by the both statistic in Fig. 3. In fact, it is the upper surface that plays a crucial role for high intensity to elongate the isolated period and to dissipate more energy.

5 OPTIMAL VALUES

The existence of an optimal value of the friction coefficient able to minimize the displacement of pier top is the result of counteracting effects that occur for increasing values of the friction coefficient as already highlighted in [23]: increase of the isolator strength with increase of the equivalent stiffness and with a reduction of the corresponding equivalent fundamental vibration period; increase of participation of higher vibration modes as well as transfer of forces towards the superstructure; increase of energy dissipation (equivalent damping).

Fig. 6 reports the variation of $\Pi^*_{\mu,optimum}$ with Π_λ and T_p for T_d = 2s (Fig. 6 a) and T_d = 3s (Fig. 6 b) obtained by considering the minimization of the median (i.e., 50th percentile) of the normalized displacement of pier top ψ_{u_p} in the range of Π^*_μ between 0 and 0.5. It is ob-

served that $\Pi^*_{\mu,optimum}$ generally increases along with Π_λ, T_p and T_d. According to Eqn. (13), the optimal friction coefficient of the upper surface can be easily calculated as $f_{1,\max,\mathrm{opt}} = \dfrac{\Pi^*_{\mu,\mathrm{opt}} \cdot S_A(T_d)}{g}$ and of lower surface since the ratio is assumed equal to 4 (Table 2). Thus, it increases linearly with the *IM* level.

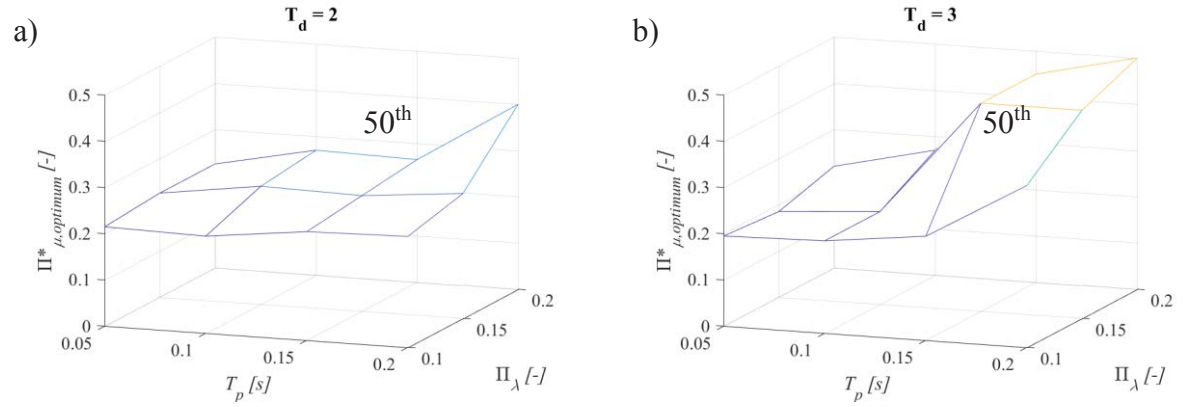

Figure 6. Critical values of normalized friction vs. Π_λ and T_p for T_d =2s (a) and T_d =3s (b).

6 CONCLUSIONS

This paper investigates the seismic performance of bridges isolated with double concave friction pendulum (DCFP) isolators considering the pier-abutment-deck interaction. They are illustrated the results of a parametric study for different isolator and bridge properties and various response parameters that are of interest for monitoring the seismic behavior. The behavior of these systems is analyzed by employing an eight-degree-of-freedom model accounting for the pier flexibility.

An ensemble of ground motions is considered to simulate the record-to-record variability effects, and a nondimensionalization of the results of the equation of motion is proposed to unveil the parameters controlling the problem.

The influence of dynamic and DCFP system properties are evaluated by considering the geometric mean (GM) and dispersion of each normalised response parameter, assumed to follow a lognormal distribution.

The results demonstrate that the increase of the normalized friction coefficient leads to a decrease of the deck response whereas the normalized response of the pier presents a particular trend showing the existence of an optimal value able to minimize this curve. The value of the optimal non-normalised friction coefficient depends on the structural properties. Specifically higher values are required for high pier period combined to high isolated deck period.

REFERENCES

[1] M. C. Constantinou, A. Kartoum, A. M. Reinhorn, P. Bradford , Sliding isolation system for bridges: Experimental study, *Earthquake Spectra* 1992; 8(3): 321-344.

[2] A. Kartoum, M. C. Constantinou, A. M. Reinhorn, Sliding isolation system for bridges:

Analytical study, *J. Struct. Eng.* 1992; 8(3): 345-372.

[3] P. Tsopelas, M. C. Constantinou, Y. S. Kim, S. Okamota, Experimental study of FPS system in bridge seismic isolation, *Earthquake Eng. Struct. Dyn.* 1996a; 25(1): 65-78.

[4] P. Tsopelas, M. C. Constantinou, S. Okamota, S. Fujii, D. Ozaki, Experimental study of bridge seismic sliding isolation systems, *Eng. Struct.* 1996b; 18(4): 301-310.

[5] A. Ghobarah, H. M. Ali, Seismic performance of highway bridges, *Eng. Struct.* 1988; 10(3): 157-166

[6] Troisi R., Alfano G. 2019. Towns as Safety Organizational Fields: An Institutional Framework in Times of Emergency. *Sustainability*, 11: 7025, 2019, doi:10.3390/su11247025.

[7] Troisi R., Alfano G. 2020. Firms'crimes and land use in Italy. An exploratory data anlysis. New Metropolitan Perspectives, International Symposium – 4th edition, 27-30 May 2020, pp 10.

[8] D. H. Turkington, A. J. Carr, N. Cooke, P. J. Moss, Seismic design of bridges on lead-rubber bearings, *J. Struct. Eng.* 1989; 115(12): 3000-3016.

[9] R. S. Jangid, Seismic response of isolated bridges, *J. Bridge Eng.* 2004; 9(2): 156-166.

[10] R. S. Jangid, Stochastic Response of Bridges Seismically Isolated by Friction Pendulum System, *J. Bridge Eng*. 2008; 13(4): (319).

[11] Y. P. Wang, L. L. Chung, W. H. Liao, Seismic response analysis of bridges isolated with friction pendulum bearings, *Earthquake Eng. Struct. Dyn.* 1998; 27(10): 1069-1093.

[12] VA. Zayas, SS. Low, SA. Mahin, A simple pendulum technique for achieving seismic isolation. *Earthquake Spectra* 1990; 6:317–33.

[13] L. Su, G. Ahmadi , IG. Tadjbakhsh, Comparative study of base isolation systems. *Journal of Engineering Mechanic* 1989; 115:1976–92.

[14] A. Mokha , MC. Constantinou, AM. Reinhorn, Teflon Bearings in Base Isolation. I: Testing. *J. Struct. Eng.* 1990; 116(2): 438-454.

[15] M. C. Constantinou, A. Mokha, A. M. Reinhorn, Teflon Bearings in Base Isolation. II: Modeling. *J. Struct. Eng*. 1990; 116(2):455-474.

[16] M. C. Constantinou, AS. Whittaker, Y. Kalpakidis, DM. Fenz, GP. Warn, Performance of Seismic Isolation Hardware Under Service and Seismic Loading. Technical Report, 2007.

[17] J. L. Almazàn, J. C. De la Llera, Physical model for dynamic analysis of structures with FPS isolators. *Earthquake Engineering and Structural Dynamics* 2003; 32:1157–1184.

[18] D. M. Fenz, M. C. Constantinou, Behaviour of the double concave friction pendulum bearing, *Earthquake Engineering and Structural Dynamics*, 2006; 35:1403-1424.

[19] M. C. Constantinou, Friction pendulum double concave bearings, technical report. University of Buffalo NY, October 29, 2004.

[20] Y. S. Kim, C. B. Yun, Seismic response characteristics of bridges using double concave friction pendulum bearings with tri-linear behavior. *Engin. Struct*. 29, 2007, 3082-3093.

[21] P. Castaldo, B. Palazzo, P. Della Vecchia, Life-cycle cost and seismic reliability analy-

sis of 3D systems equipped with FPS for different isolation degrees, *Engineering Structures*, 2016; 125: 349–363.

[22] P. Castaldo, G. Amendola, B. Palazzo , Seismic fragility and reliability of structures isolated by friction pendulum devices: Seismic reliability-based design (SRBD), *Earthquake Engineering and Structural Dynamics*, 2017, 46(3); 425–446, DOI: 10.1002/eqe.2798.

[23] P. Castaldo, M. Ripani, R. Lo Piore, Influence of soil conditions on the optimal sliding friction coefficient for isolated bridges, *Soil Dynamics and Earthquake Engineering*, 2018, 111; 131–148, https://doi.org/10.1016/j.soildyn.2018.04.056.

[24] Y. P. Wang, L. Chung, H. L. Wei, Seismic response analysis of bridges isolated with friction pendulum bearings, *Earthquake Eng. Struct. Dyn.*, 27(10); 1069-1093.

[25] E. Tubaldi E, L. Ragni, A. Dall'Asta, Probabilistic seismic response assessment of linear systems equipped with nonlinear viscous dampers, *Earthquake Engineering & Structural Dynamics* 2014; DOI: 10.1002/eqe.2461.

[26] P. Castaldo, E. Tubaldi, Influence of FPS bearing properties on the seismic performance of base-isolated structures, *Earthquake Engineering & Structural Dynamics*, 2015; 44(15): 2817-2836.

[27] P. Castaldo, M. Ripani, Optimal design of friction pendulum system properties for isolated structures considering different soil conditions, *Soil Dynamics and Earthquake Engineering*, 2016, 90:74–87, DOI: 10.1016/j.soildyn.2016.08.025.

[28] P. Castaldo, E. Tubaldi, Influence of ground motion characteristics on the optimal single concave sliding bearing properties for base-isolated structures. *Soil Dynamics and Earthquake Engineering*, 2018, 104: 346–364.

[29] RD. Bertero, VV. Bertero, Performance-based seismic engineering: the need for a reliable conceptual comprehensive approach. *Earthquake Engineering and Structural Dynamics,* 2002;31:627–652 (DOI: 10.1002/eqe.146).

[30] H. Aslani, E. Miranda, Probability-based seismic response analysis. *Engineering Structures* 2005; **27**(8): 1151-1163.

[31] P. Castaldo, B. Palazzo, T. Ferrentino T., Seismic reliability-based ductility demand evaluation for inelastic base-isolated structures with friction pendulum devices, *Earthquake Engineering and Structural Dynamics*, 2017, 46(8): 1245-1266, DOI: 10.1002/eqe.2854.

[32] Castaldo P., Alfano G. Seismic reliability-based design of hardening and softening structures isolated by double concave sliding devices, *Soil Dynamics and Earthquake Engineering*, 129: 105930, 2020.

[33] P. Castaldo, B. Palazzo, G. Alfano, MF. Palumbo, Seismic reliability-based ductility demand for hardening and softening structures isolated by friction pendulum bearings, 2018, *Structural Control and Health Monitoring*, e2256. https://doi.org/10.1002/stc.2256.

[34] N. Shome, C. A. Cornell, P. Bazzurro, J. E. Carballo, Earthquake, records, and nonlinear responses. *Earthquake Spectra*, 1998, 14(3); 469-500.

[35] N. Luco, C. A. Cornell, Structure-specific scalar intensity measures for near-sorce and ordinary earthquake ground motions. *Earthquake Spectra*, 2007, 23(2); 357-392.

[36] Garzillo C., Troisi R. Le decisioni dell'EMA nel campo delle medicine umane. In EMA e le relazioni con le Big Pharma - I profili organizzativi della filiera del farmaco, G. Giappichelli, 85-133, 2015.

[37] Golzio L. E., Troisi R. The value of interdisciplinary research: a model of interdisciplinarity between legal re-search and research in organizations. *Journal For Development And Leadership*, 2: 23-38, 2013.

[38] Nese A.; Troisi R. Corruption among mayors: evidence from Italian Court of Cassation judgments, *Trends In Organized Crime*, 1-26, 2018. DOI:10.1007/s12117-018-9349-4.

[39] Troisi R., Golzio, L. E. Legal studies and organization theory: a possible cooperation. *Manageable cooperation* - European Academy of Management: 16th EURAM Conference, Paris, 1-2, 1-4 June 2016.

[40] Troisi R., Guida V. Is the Appointee Procedure a Real Selection or a Mere Political Exchange? The Case of the Italian Health-Care Chief Executive Officers. *Journal of Entrepreneurial and Organizational Diversity*, 7 (2): 19-38, 2018, DOI:10.5947/jeod.2018.008.

[41] Troisi R. Le risorse umane nelle BCC: lavoro e motivazioni al lavoro. In Progetto aree bianche. Il sistema del credito cooperativo in Campania, 1: 399-417, 2012.

[42] Math Works Inc. MATLAB-High Performance Numeric Computation and Visualization Software. User's Guide. Natick: MA, USA, 1997.

[43] Castaldo, P., Gino, D., Bertagnoli, G. & Mancini, G. Resistance model uncertainty in non-linear finite ele-ment analyses of cyclically loaded reinforced concrete systems, *Engineering Structures*, 211: 110496, 2020, https://doi.org/10.1016/j.engstruct.2020.110496.

[44] P. Castaldo, D. Gino, G. Mancini, Safety formats for non-linear analysis of reinforced concrete structures: discussion, comparison and proposals. *Engineering Structures*, 193,136-153, 2019.

[45] P. Castaldo, D. Gino, G. Bertagnoli, G. Mancini, Partial safety factor for resistance model uncertainties in 2D non-linear finite element analysis of reinforced concrete structures. *Engineering Structures,* 176:746-762, 2018.